Triple point of Lennard-Jones fluid in slit nanopore: Solidification of critical condensate

Hideki Kanda
Chemical Energy Engineering Department, Central Research Institute of Electric Power Industry,
2-6-1 Nagasaka Yokosuka Kanagawa 240-0196, Japan

Minoru Miyahara and Ko Higashitani
Department of Chemical Engineering, Kyoto University, Kyoto 615-8510, Japan

We report the results of a molecular dynamics simulation that looked for the triple point of Lennard-Jones fluid in slit-shaped nanopores. The simulation method employed for this purpose is able to maintain vapor–liquid coexistence in a nanopore at a specific equilibrium bulk-phase pressure. The triple point is the freezing point of the critical condensate. The triple-point temperature could be higher or lower than the bulk triple point, depending on the pore size. This is thought to be due to two opposing factors: the elevating effect of the pore-wall potential energy, and the depressing effect of the capillary condensate's tensile condition. Because of the cancellation, the deviation of the triple-point temperature from the bulk triple-point temperature was not considered significant. The pressure of the triple point, however, was significantly different from that of the bulk triple point. A simple model to describe the triple point is developed and shown to agree well with the results of the simulation. The importance of the two factors in nanoscale pores, which cannot be described by the classic Gibbs–Thomson equation, is emphasized. © *2004 American Institute of Physics.* [DOI: 10.1063/1.1652431]

I. INTRODUCTION

Solidification in pores has been extensively studied experimentally.[1–10] Most of these studies report a decrease in freezing point and confirm the reliability of the Gibbs–Thomson equation,[11] which shows a linear relationship between the shift in freezing point and the reciprocal pore size. The equation for the simplest geometry of the confining space, a slit pore, is as follows:

$$T_f - T = \frac{2\gamma_{sl}T_f}{H\Delta h_m} v_S \cos\theta, \tag{1}$$

where H is pore width, Δh_m the latent heat of melting for the bulk phase, T_f the normal freezing point, γ_{sl} the solid–liquid interfacial tension, v_S the volume per molecule of the bulk solid, and θ the contact angle of the solid–liquid interface against the wall. According to Eq. (1), only the excess energy of the solid–fluid interface contributes to the decrease in the freezing point, and the freezing point must be independent of the vapor pressure in the bulk phase. However, some recent experimental studies report an inexplicable elevation of the freezing point.[12,13] Moreover, recent molecular simulation studies by some research groups, including us, have revealed the inadequacies of the Gibbs–Thomson equation, especially at the nanometer scale.

The freezing phenomena in confined spaces must be affected, we suppose, by at least the following three effects: (i) the strength of pore-wall potential energy (compression effect), (ii) the geometrical shape of pore (geometrical hindrance), and (iii) the equilibrium vapor-phase pressure (tensile effect). Molecular simulation techniques are appropriate

for clarifying the contribution of each, while experimental measurements may suffer from the combined effects of the above factors and others.

The following aspects of the first effect[14] were clarified by conducting the grand canonical Monte Carlo (GCMC) simulations of Lennard-Jones (LJ) fluids in slit pores. Depending on the strength of the attractive potential energy from the pore walls, the fluid in a slit pore in equilibrium with saturated vapor shows elevation as well as depression of the freezing point, and the critical strength dividing these two cases was the potential energy exerted by the fluid's solid state. The ''excess'' attraction relative to the critical one was thought to bring the confined liquid to a higher-density state that resembles a compressed state, which would result in the elevated freezing point.

These results agree well with those of other recent studies. Dominguez *et al.*[15] examined the freezing of LJ fluid in slit pores with purely repulsive and weakly attractive walls, employing thermodynamic integral techniques to determine the true equilibrium points. The freezing points, rigorously determined by free-energy calculation, showed a significant downward shift relative to the bulk in purely repulsive walls, while the downward shift was much smaller in magnitude in weakly attractive walls. Radhakrishnan and Gubbins[16] used a different approach to determine the freezing point in slit pores, employing the Landau free energy calculation. They showed that a simple fluid in strongly attractive slit pores has elevated freezing points, not only theoretically but also experimentally, as reported in other papers.[17,18]

As for the second effect, the freezing behavior of a LJ fluid confined in cylindrical pores was investigated by the

authors employing GCMC simulations.[19] With the saturated vapor for the equilibrium bulk condition, the fluid confined in a cylindrical pore had a lower freezing point than that in a slit pore with the same attractive potential energy, and the lowering was more significant for smaller pores. The lowering of the freezing temperature, relative to the slit pore, was interpreted as the result of the difficulty in forming an ordered molecular arrangement within the circular pore space, which we called "geometrical hindrance." A fluid in a cylindrical pore with strong attraction is subject to the two competing effects on the freezing point—the elevation by the compression effect and the depression by the geometrical hindrance—and exhibits nonmonotonic variation of the freezing point relative to the pore diameter. Cylindrical pores with relatively weak potential energy, however, display monotonic depression of the freezing point relative to the pore size. This is in line with the long-observed depression in experimental studies that used materials with roughly cylindrical pores. The lower freezing point in pores with a cylindrical geometry other than a slit is in qualitative agreement with the results of molecular dynamics (MD) simulation studies by Maddox and Gubbins.[20]

The third effect—equilibrium vapor-phase pressure p—was also examined by the authors[21] for the following reason. Contrary to the case with saturated vapor p_s (the equilibrium bulk-phase pressure condition), the capillary-condensed liquid with $p/p_s < 1$ is subjected to far lower pressure than it is in the equilibrium bulk-phase pressure condition. Negative pressure, or a tensile condition, can occur easily in liquids in nanopores, an effect that should depress the freezing point. MD simulations have found liquid–solid phase transitions at a constant temperature and with the variation in the equilibrium vapor-phase pressure below that of the saturated phase. In this way, on a $p-T$ diagram, the determined solid–liquid coexistence line exhibited significant dependence on the freezing point vs small changes in the bulk-phase vapor pressure. This is in contrast to the bulk-phase coexistence of an almost vertical line, and illustrates the importance of the tensile effect on freezing in nanopores. The origin of the skew was proved to be the tensile effect in capillary condensed phase, as shown by studies using a new model based on this effect.

While our understanding and modeling of the freezing in slit pores has been advancing in this way, the capillary condensation phenomena in nanospace, or gas–liquid coexistence, has also been studied recently by many researchers, including us.[22–26] Using the Kelvin equation ensured misleading estimations of nanoscale pore sizes, so a simple model was developed to overcome the failure. However, there is little understanding about the triple point in pores, which should serve to connect the above two coexistence lines.

Following the above studies concerning phase coexistence relations in nanopores, this study examined the triple points of pore fluids. We employed a MD technique in a unit cell with an imaginary gas phase developed by the authors.[22] This enabled us to set or obtain the equilibrium vapor-phase pressure for the adsorbed phase. Fluid is kept in a pore sufficiently long to remain in the critical condensation condi-
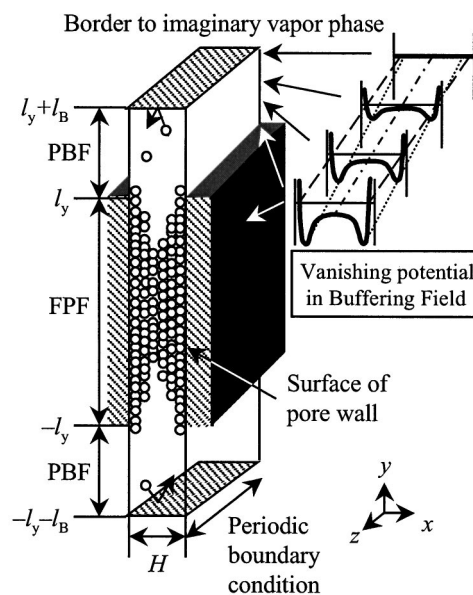

FIG. 1. Schematic figure of unit cell and potential profile within the cell. The full potential energy in FPF attenuates in PBF to vanish at the border.

tion, and is then simulated at various temperatures. The solid–liquid transition of the critical condensate, which *is* the triple point, is thus determined for various pore widths. Our model of the triple point, or the simultaneous solution of our model of vapor–liquid coexistence[23,24] and that of solid–liquid coexistence,[21] successfully predicts the simulation results with no need to introduce any adjustable parameters, and thus proves its reliability.

II. MD SIMULATION WITH IMAGINARY GAS PHASE

The strategy for finding the triple points of pore fluid is as follows. Basically, NVT-MD simulation is carried out. We keep a capillary condensate with an appropriate number of molecules in a sufficiently long pore space, which automatically maintains the capillary coexistence condition. The temperature is gradually lowered from one simulation run to another, and the condition of the pore fluid is checked during this series of simulation runs at various temperatures. When the fluid freezes, it indicates that the system has passed the triple point temperature, because the freezing point of the critical condensate *is* the triple point for a given pore space.

If a normal simulation cell is employed, we may encounter some difficulty in knowing the condition of the bulk equilibrium vapor phase. This study used the unit cell shown in Fig. 1. We originally developed it in order to more easily obtain the equilibrium vapor-phase pressure. For details of the cell, please refer to the authors' previous papers[21,22] as only an outline is provided below. In the middle of the cell, the pore space was given a specific potential field [full potential field (FPF)]. The pore fluid stays within the FPF in order to produce the capillary coexistence condition. At each end of the cell, at a sufficient distance from the edge of the FPF, we established a border plane beyond which an imaginary gas phase is assumed to exist. Since the external energy in the gas phase must be zero, there should exist a connecting space with a slope of potential energy between the vapor

phase and the pore space [potential buffering field (PBF)]. Some of molecules escaping from the FPF may reach the border plane if they have sufficient kinetic energy to overcome the slope in the PBF. With a perfect reflecting condition at the border, the frequency reached by the molecules must be a direct measure of the vapor pressure in bulk that is in equilibrium with the given adsorbed phase. The equilibrium vapor phase pressure can then be calculated by counting the number of rebounds at the border over a certain period of time.

The fluid employed is a truncated and shifted LJ fluid modelled on methane ($\epsilon_{ff}/k = 148.1$ K, $\sigma_{ff} = 0.381$ nm), with the cut-off distance of $5\sigma_{ff}$, which is felt to be large enough to represent particles with the full LJ potential. The mass is 2.664×10^{-26} kg. The structureless 10-4-3 potential for graphite[27,28] was employed for each pore wall. Lorentz–Berthelot combining rules were applied to obtain parameters for the methane–carbon interactions. The pore width H was from $5.5\sigma_{ff}$ to $10.0\sigma_{ff}$. The potential energy in the pore space (FPF), ψ, was calculated as the sum of the contribution from the two walls: $\psi(x) = \phi(H/2-x) + \phi(H/2+x)$. The length of the wall $2l_y$ was $7H$, which is long enough to accommodate thick condensates. The PBF was set to a length of $13.12\sigma_{ff}$ (5 nm), in which ψ was attenuated linearly towards zero at the border of the imaginary gas phase. The z-direction size of the cell was $10\sigma_{ff}$, under period boundary conditions. The number of particles N for a given pore width was chosen to be sufficient for making a condensate with a thickness of ≈ 10 nm ($\approx 26\sigma_{ff}$).

The first run was started for a given N from an initial configuration arranged as a liquidlike phase at a higher temperature. The duration of each run was decided so that the number of particles reaching the border plane was about 500 or more, which resulted in a typical simulation time of 10–150 ns. The last configuration, at a higher temperature, was the initial configuration at a lower temperature. Since the system automatically traces the gas–liquid coexistence in the pores, the freezing point in this sequence *is* the triple point for a given pore size. The freezing points in the pores were determined from discrete changes in the density and arrangement of particles at various temperatures. For further details about the calculation, please refer to our previous paper.[21]

As for the hysteresis, different transition temperatures in the cooling/heating sequence inevitably occur in this simulation cell, but to a much smaller extent than in GCMC simulations. Furthermore, as reported earlier,[14,21] the freezing branch was considered closer to the true transition point than was the melting sequence. In this study, we are mainly interested in the freezing points in the cooling sequence.

III. RESULTS AND DISCUSSION

A. Liquid–solid phase transition of critical condensate

Figure 2 shows a typical side view of LJ-methane in graphite pores of $H^* = 9.5$ at various temperatures. It is worth noting that the condensed phase stays within the limited portion of the pore space that has full potential energy (FPF), and the gas phase coexists with the condensed phase
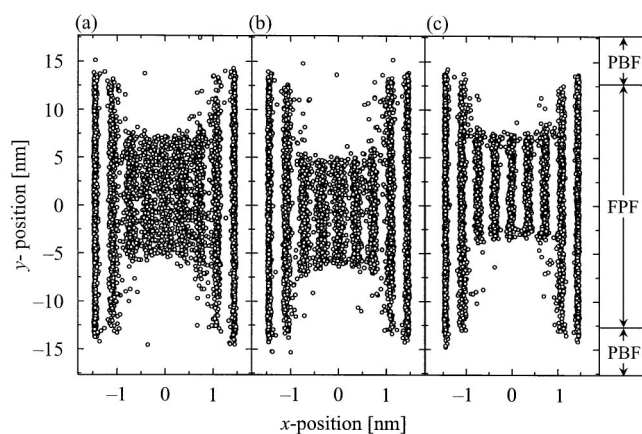

FIG. 2. Snapshots of critical condensates within a pore of $H/\sigma_{ff} = 9.5$: (a) $T = 111.4$ K, (b) $T = 105.8$ K, (c) $T = 105.0$ K.

in FPF. The system maintains the critical condensation condition. At a higher temperature [Fig. 2(a)], the pore fluid exhibits a liquidlike structure with a small degree of layering. This is typically observed for capillary condensate in a pore with a width of a few nanometers. Note that the x-scale of each figure is expanded in order to more easily recognize the layers. At 105.8 K, the degree of layering becomes more recognizable [Fig. 2(b)], but some molecules still exist between the inner layers. Only a slight cooling down to 105.0 K, a 0.8 K reduction, brings about the solidlike state seen in Fig. 2(c), where the discrete distribution can be clearly recognized.

The above difference between Fig. 2(b) and Fig. 2(c) might appear subtle, but in-plane snapshots of the innermost layer show a definite difference between the two states, as shown in Fig. 3. A liquidlike structure of random nature at 105.8 K becomes a completely ordered structure with a hexagonal array at 105.0 K. Note that the contact layer adjacent to the pore wall does not participate in the phase transition. Rather, it maintains its hexagonal order before and after the change. This is similar to the behavior observed in GCMC for systems under equilibrium with saturated vapor.[14]

The transition is quantitatively examined with the overall density ρ^* of the adsorbate. For the condition in which the pore fluid freezes, a slight amount of melted phase inevitably exists around the edges of the frozen phase due to the somewhat parallel case of so-called "surface melting." The density of a central portion of the FPF (CFPF) that has a
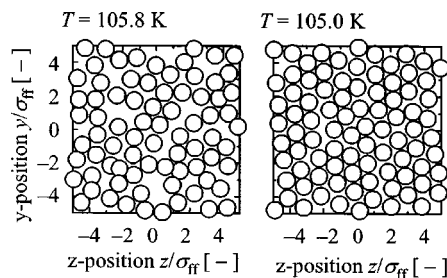

FIG. 3. In-plane snapshots for the innermost layer in a pore of $H/\sigma_{ff} = 9.5$: the left figure corresponds to Fig. 2(b), and the right to Fig. 2(c).
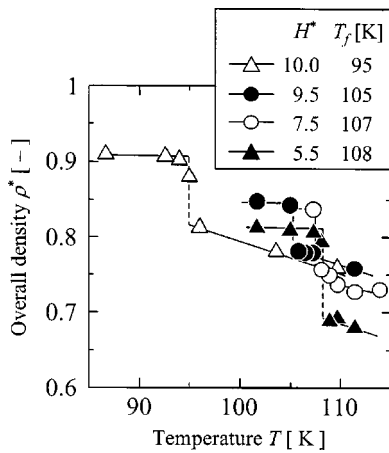
FIG. 4. Overall density of critical condensates on cooling. Stepwise changes in density at the tabulated temperatures indicate the transition.

FIG. 5. MD results of $p-T$ relation for the pore of $H/\sigma_{ff}=9.5$ superimposed on bulk phase boundaries (broken lines). Open circles show the liquid state, and closed circles the solid state. Also drawn are estimated phase boundaries for pore fluids (solid lines) explained in Sec. III B.

length of $10\sigma_{ff}$ and is free of melted molecules is calculated in a manner similar to that used in the previous study,[21]

$$\rho^* = \rho\sigma_{ff}^3: \quad \rho = \frac{\langle N \rangle}{V} \quad \text{and} \quad V = H \times 10\sigma_{ff} \times 10\sigma_{ff}, \quad (2)$$

where $\langle N \rangle$ is the ensemble average of the number of particles in the CFPF. V is the volume of the CFPF between the nuclei of the carbon atoms on the wall surface and includes some dead space near the wall, which methane cannot penetrate. For smaller pores, this region forms a larger fraction of the total volume, thus giving a smaller apparent density. Figure 4 shows variation of overall density in CFPF versus temperature for various pore sizes. In the higher temperature range, the density shows a gradual increase upon cooling. At triple points, a discrete change in density occurs, which must be attributed to the rearrangement of the molecules. Below this temperature, almost no variation in density is observed with further cooling.

These observations clearly demonstrate that the discrete changes are associated with the liquid–solid phase transition. Furthermore, though not shown here, we calculated the in-plane pair correlation functions and the static structure factors for the individual layers. All results support the idea that the steplike changes versus temperature are transitions from a disordered liquidlike state to an ordered solidlike state. These functions show a manner of change quite similar to that observed when freezing pore fluid is in equilibrium with saturated vapor in the bulk phase.[14] Since the system automatically traces the gas–liquid coexistence curve for pore fluid, the observed freezing point is the triple point for a given pore size.

The obtained data series are plotted on a $p-T$ diagram together with the bulk phase coexistence curves in Fig. 5 for a pore of $H^*=9.5$ as an example. (The figure also plots phase coexistence curves for pore fluid, which will be explained in the next section.) Thus, the triple point was determined to be $T=105.0$ K, $p/p_s=0.326$ ($p=0.186$ atm) for this pore size, as compared to that for bulk fluid, $T=101$ K, $p=0.41$ atm. The obtained triple-point temperature for this pore is not significantly different from that for bulk fluid. As shown previously,[14] the freezing point for pore fluid
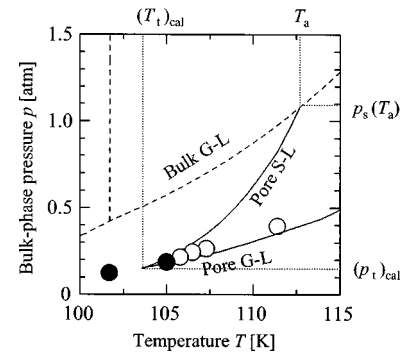
in equilibrium with saturated vapor in bulk is around 110 K, which is elevated from the bulk value by the compression effect of the pore-wall attraction potential. This effect, however, is considered to be cancelled out to a certain extent by the depressing effect originating from the tensile condition in the capillary condensate. The pressure at the triple point, however, is significantly different from that of the bulk fluid.

B. Simple model

As mentioned earlier, the authors proposed a model of solid–liquid coexistence under tensile condition (with the condition of $p/p_s<1$).[21] In addition, a series of studies by the authors proposed a model of vapor–liquid coexistence (capillary condensation) in nanopores,[22–26] whose characteristics were nonuniform in the curvature of the gas-condensate interface, as explained below. For the sake of convenience, we call this the nonuniform curvature (NUC) model. The simultaneous application of the two models should give the triple point for comparison with the simulation results. The concept and brief descriptions of the models are provided below.

In the NUC model, the attractive potential from the pore walls is included as a contribution to the condensation equilibrium. This is in addition to the Young–Laplace effect. The basic equation of the condensation model is as follows:

$$kT\ln\frac{p}{p_s} = \Delta\psi(x) - v_L\frac{\gamma_{gl}}{\rho(x)}, \quad (3)$$

where k is the Boltzmann constant and v_L the volume per molecule of the condensate, which can be approximated from that for bulk liquid. $\rho(x)$ is the local radius of the curvature of the gas-condensate interface at position x in the pore space (taken as a positive value). $\gamma_{gl}(\rho)$ is the surface tension of the liquid, which is treated as a function of the curvature. The relation given by the Gibbs–Tolman–Koenig–Buff equation[29–32] is used for the dependence. $\Delta\psi(x)$ is the contribution of the attractive potential energy from pore walls, which must be expressed as an "excess" amount compared with the potential energy that a molecule would feel if the pore walls consisted of the same molecules as the adsorbate. The curvature becomes location-dependent and nonuniform because of this contribution by the pore-wall

potential. Based on Eq. (3), the local curvature can be calculated for every position within the pore, and its geometrical integration will determine the "core" size of the condensate, which will give the pore size if summed with the thickness of the adsorbed film on the interior surface of the pore.

For a fair examination of the model, the physical properties to be used in the model must be those for a LJ fluid with the same cut-off distance employed in the simulation. The surface tension and Tolman's length are properties known to be quite sensitive to the cut-off distance. We conducted MD simulations of liquid slabs to obtain these properties as a function of temperature, the details of which are described in the Appendix.

The other model describing solidification of tensile capillary fluid with the bulk condition of $p/p_s < 1$ was based on the following concept:[21]

(i)   Introducing an effective pressure for pore fluid, p^{pore}, the solid–liquid coexistence line with respect to this pressure follows the Clapeyron equation, the slope of which can be approximated by using that for bulk fluid,

$$\frac{dp^{pore}}{dT} = \left(\frac{\Delta s}{\Delta v}\right)_{pore} \cong \left(\frac{\Delta s}{\Delta v}\right)_{bulk} \cong \text{const.} \qquad (4)$$

(ii)   The variation in p^{pore} relative to the starting point of the solid–liquid coexistence line of pore fluid (freezing point of pore fluid in equilibrium with saturated vapor in bulk) is

$$\Delta p^{pore} \cong \frac{kT}{v_L} \ln \frac{p}{p_s(T)}. \qquad (5)$$

(iii)   The combination of the above two equations and simple integration gives a relation describing the solid–liquid coexistence line $p = p(T)$,

$$p = p_s(T) \exp\left[-\left(\frac{\Delta s}{\Delta v}\right)_{bulk} \frac{v_L}{kT}(T_a - T)\right], \qquad (6)$$

where T_a is the freezing temperature of pore fluid in equilibrium with saturated vapor $p_s(T_a)$ in bulk, which can be predicted by the equation proposed by Miyahara and Gubbins.[14] Equation (6) gives solid–liquid coexistence (p,T) with unsaturated vapor-phase pressure when T_a is given.

Using physical properties of bulk LJ fluid, the phase boundaries for the pore fluid are calculated by the above two models as described in Fig. 5. The dashed curves are coexistence lines of the LJ methane for the bulk phase that were calculated from Kofke and Agrawal's phase diagram.[33,34] The solid lines are predictions from the NUC model and the freezing model for tensile fluid. Note that the model predictions do not include any fitting parameter. For the pore of $H/\sigma_{ff} = 9.5$, e.g., the intersection of the two curves is located at $T = 104.1$ K, $p/p_s = 0.319$ ($p = 0.168$ atm), and agrees well with the MD simulation result.

Calculations for other pore sizes are conducted in the same way. The results are shown in Figs. 6(a)–6(c). Although there are 1 or 2 K discrepancies in the triple-point temperature, the model prediction quite successfully describes the behavior of the triple point on the p–T diagram.
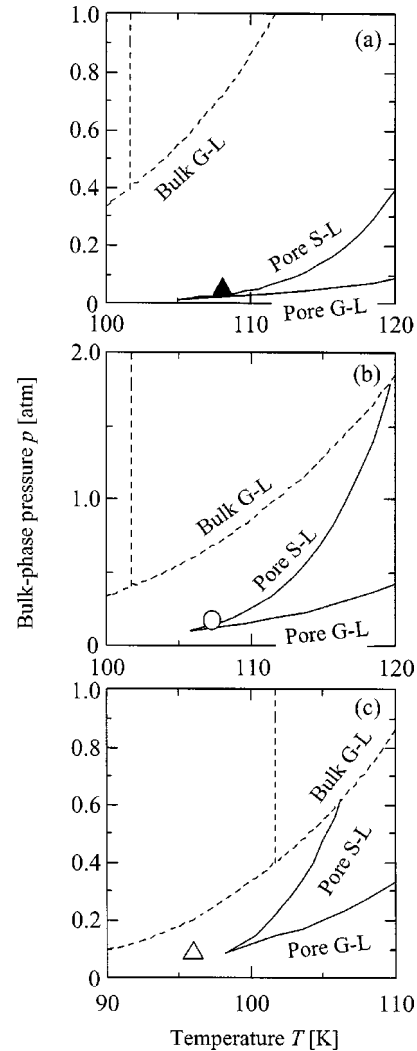

FIG. 6. Comparison of triple points observed in simulations (keys) and the estimates by the two models of solid–liquid and gas–liquid phase coexistence for each pore size (solid lines). The intersection of the two coexistence lines should give the triple point. (a) $H/\sigma_{ff} = 5.5$; (b) $H/\sigma_{ff} = 7.5$; (c) $H/\sigma_{ff} = 10.0$.

As the result of the complicated influence both by the pore-wall potential and the tensile effect, the triple point can be higher or lower than the bulk triple point, and the triple-point pressure becomes far lower than that of the bulk fluid. It is surprising that the models with such a simple concept were able to successfully express phase behavior in nanoscale pores. This agreement would be proof of the usefulness of the concept of *effective pressure felt by the pore fluid*, in understanding the freezing phenomena in nanopores.

C. Relevance of the Gibbs–Thomson equation

The relevance of the Gibbs–Thomson equation is based on the above models. Combining the two models, or Eqs. (3) and (6), we formally obtain an expression for the triple point in pore, T_t^{pore},

$$T_t^{pore} - T_a = \left(-\frac{\gamma_{gl}}{\rho(x)} + \frac{\Delta \psi}{v_L}\right)\left(\frac{\Delta v}{\Delta s}\right)_{bulk}. \qquad (7)$$

An important feature of the above equation is that it agrees with the Gibbs–Thomson equation only for large pore sizes, where the effect of the pore-wall potential disappears. With this condition of $\Delta\psi=0$, the freezing point in equilibrium with saturated vapor, T_a, will drop to the triple point for bulk phase T_t^{bulk}. Moreover, curvature ρ will remain constant and equal to $2/H$. Then Eq. (7) reduces to

$$T_t^{\text{pore}} - T_t^{\text{bulk}} = -\frac{2}{H(\Delta s)_{\text{bulk}}}(\Delta v)_{\text{bulk}}\gamma_{\text{gl}}. \tag{8}$$

On the other hand, the Gibbs–Thomson equation [Eq. (1)] can be rewritten as

$$T_f^{\text{pore}} - T_f^{\text{bulk}} = -\frac{2}{H(\Delta s)_{\text{bulk}}}(v_s)_{\text{bulk}}\gamma_{\text{sl}}\cos\theta. \tag{9}$$

Eventually, the two equations give almost identical results. This is because the portions dealing with molar volume and interfacial tension, which may look different, produce quite similar figures in most cases due to the often encountered relations of $\Delta v \cong 0.1 v_s$, $\gamma_{\text{sl}} \cong 0.1-0.2\gamma_{\text{gl}}$, and $\cos\theta \cong 0.5-1.0$. This agreement and the success of present model at the nanoscale level show that the Gibbs–Thomson equation may hold true for larger pores but NOT nanoscale pores, where the compression effect of the pore-wall potential and the strong capillary tensile effect produced by the equilibrium vapor-phase pressure have considerable effect on the freezing phenomena.

IV. CONCLUSION

Triple points in nanopores were examined by employing a MD technique that was able to maintain the vapor–liquid coexistence condition at the specified bulk equilibrium pressure. This technique successfully determined the triple points in nanopores located on the bulk phase diagram. The triple-point temperatures can be higher or lower than the bulk triple point depending on the pore size, which was thought to have resulted from the complicated influence of both the elevating effect produced by the strongly attractive pore-wall potential energy and the depressing effect that originates from the tensile condition in the capillary condensate. Because of the cancellation, the deviation of the triple-point temperature from the bulk was not significant, staying within 10 K. The pressure of the triple point, however, exhibited significant difference from the bulk.

A simple model to describe triple points was derived by combining condensation and freezing models described by the authors in previous studies. The model showed good agreement with the MD results and proved to be reliable. The importance of the two factors in nanoscale pore was emphasized, which cannot be described by the classic Gibbs–Thomson equation.

APPENDIX: PHYSICAL PROPERTIES OF THE MODEL FLUID

To test the present model, some physical properties of the model adsorbate employed in the simulations must be known. These properties include the saturated vapor pressure, the volume per molecule, the freezing point, the gas–
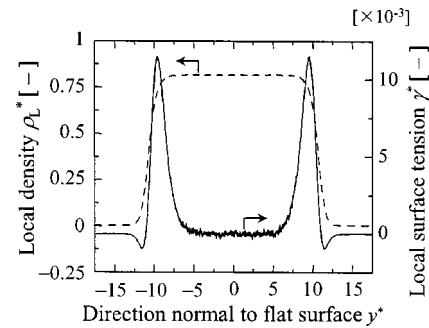

FIG. 7. Local density and local surface tension of liquid film at 109.7 K.

liquid surface tension, and the distance between the equimolar dividing surface and the surface of tension, δ (Tolman's length or dividing thickness) within the interfacial region—all for the bulk liquid state of LJ-methane with a cut-off distance of $5\sigma_{ff}$. Tolman's length and the surface tension are quite sensitive to the cut-off distance and temperature. Therefore, using the MD method, we simulated a liquid film consisting of an adsorbate fluid in a rectangular cell.

We set up a system of 7000 particles in a box of dimensions $L_x \times L_y \times L_z = 20.0\sigma_{ff} \times 52.5\sigma_{ff} \times 20.0\sigma_{ff}$ following the literature.[35–39] Similar to simulations in a pore, a border plane with an imaginary gas phase was placed vertically at each the end of the cell with sufficient distance from the liquid film. The run consisted of 1.2×10^6 integration steps of 10 fs. The saturated vapor pressure was determined by the particle counting method.

The local surface tension was calculated for a slice spacing of $L_x \times 0.0262\sigma_{ff} \times L_z$ with the following statistical mechanical expression:

$$\gamma = \frac{1}{2L_xL_z}\left\langle \sum_{i \neq j} \frac{r_{ij}^2 - 3y_{ij}^2}{r_{ij}}\frac{du(r_{ij})}{dr_{ij}}\right\rangle. \tag{A1}$$

The surface tension was a half of summation of the local surface tension over the interfacial region.[36]

Each property was determined by a running average of 2×10^5 to 1.2×10^6 steps. The local density and the local surface tension are shown in Fig. 7. Figure 8 shows two properties related to surface tension versus temperature. Using these properties, the curvature-dependent surface tension employed in the NUC model for condensation can be calculated with the following equation (where ρ is a positive value),
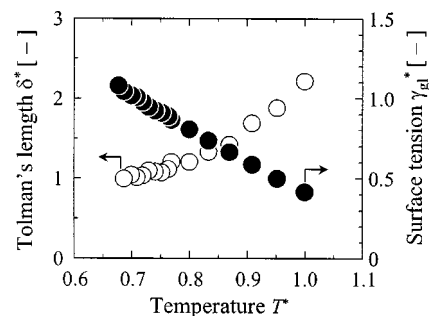

FIG. 8. Dependencies of two properties on temperature: closed circles show surface tension and open circles Tolman's length.

J. Chem. Phys., Vol. 120, No. 13, 1 April 2004

Triple point of a fluid in slit nanopore   6179

$$\gamma_{gl}(\rho) = \gamma_{\infty}(1 + \delta/\rho). \qquad (A2)$$

The temperature–pressure–density relation was confirmed to be almost identical to that of Kofke's phase diagram[23,24] with a slight difference of 3%.

[1] W. A. Patrik and W. A. Kemper, J. Phys. Chem. **42**, 369 (1938).
[2] G. K. Rennie and J. Clifford, J. Chem. Soc., Faraday Trans. 1 **73**, 680 (1977).
[3] J. L. Tell and H. J. Maris, Phys. Rev. B **28**, 5122 (1983).
[4] J. Warnock, D. D. Awschalom, and M. W. Shafer, Phys. Rev. Lett. **57**, 1753 (1986).
[5] R. H. Torii, H. J. Maris, and G. M. Seidel, Phys. Rev. B **41**, 7167 (1990).
[6] P. E. Sokol, W. J. Ma, K. W. Herwig, W. M. Snow, Y. Wang, J. Koplik, and J. R. Banavar, Appl. Phys. Lett. **61**, 777 (1992).
[7] J. H. Strange, M. Rahman, and E. G. Smith, Phys. Rev. Lett. **71**, 3589 (1993).
[8] K. M. Unruh, T. E. Huber, and C. A. Huber, Phys. Rev. B **48**, 9021 (1993).
[9] E. Moltz, A. P. Y. Wong, M. H. W. Chan, and J. R. Beamish, Phys. Rev. B **48**, 5741 (1993).
[10] J. A. Duffy, N. J. Wilkinson, H. M. Fretwell, M. A. Alam, and R. Evans, J. Phys.: Condens. Matter **7**, L713 (1995).
[11] R. Defay, I. Prigogine, and A. Bellemans, *Surface Tension and Adsorption* (Wiley, New York, 1966).
[12] J. Klein and E. Kumacheva, Science **269**, 816 (1995).
[13] S. E. Donnelly, R. C. Birtcher, C. W. Allen, I. Morrison, K. Furuya, M. Song, K. Mitsuishi, and U. Dahmen, Science **296**, 507 (2002).
[14] M. Miyahara and K. E. Gubbins, J. Chem. Phys. **106**, 2865 (1997).
[15] H. Dominguez, M. P. Allen, and R. Evans, Mol. Phys. **96**, 209 (1999).
[16] R. Radhakrishnan and K. E. Gubbins, Mol. Phys. **96**, 1249 (1999).
[17] R. Radhakrishnan, K. E. Gubbins, A. Watanabe, and K. Kaneko, J. Chem. Phys. **111**, 9058 (1999).
[18] R. Radhakrishnan, K. E. Gubbins, and M. Sliwinska-Bartkowiak, J. Chem. Phys. **112**, 11048 (2000).
[19] H. Kanda, M. Miyahara, and K. Higashitani, Langmuir **16**, 8529 (2000).
[20] M. W. Maddox and K. E. Gubbins, J. Chem. Phys. **107**, 9659 (1997).
[21] M. Miyahara, H. Kanda, M. Shibao, and K. Higashitani, J. Chem. Phys. **112**, 9909 (2000).
[22] M. Miyahara, T. Yoshioka, and M. Okazaki, J. Chem. Phys. **106**, 8124 (1997).
[23] T. Yoshioka, M. Miyahara, and M. Okazaki, J. Chem. Eng. Jpn. **30**, 274 (1997).
[24] M. Miyahara, H. Kanda, T. Yoshioka, and M. Okazaki, Langmuir **16**, 4293 (2000).
[25] H. Kanda, M. Miyahara, T. Yoshioka, and M. Okazaki, Langmuir **16**, 6622 (2000).
[26] H. Kanda, M. Miyahara, and K. Higashitani, Langmuir **16**, 6064 (2000).
[27] W. A. Steele, Surf. Sci. **36**, 317 (1973).
[28] W. A. Steele, *The Interaction of Gases with Solid Surface* (Pergamon, Oxford, 1974).
[29] R. C. Tolman, J. Chem. Phys. **16**, 758 (1948); **17**, 118 (1949); **17**, 333 (1949).
[30] J. G. Kirkwood and F. P. Buff, J. Chem. Phys. **17**, 338 (1949); **18**, 991 (1950).
[31] K. O. Koenig, J. Chem. Phys. **17**, 338 (1949); **18**, 991 (1950).
[32] J. C. Melrose, Ind. Eng. Chem. **60**, 53 (1968).
[33] D. A. Kofke, J. Chem. Phys. **98**, 4149 (1993).
[34] R. Agrawal and D. A. Kofke, Mol. Phys. **85**, 43 (1995).
[35] G. A. Chapela, G. Saville, S. M. Thompson, and H. S. Rowlinson, J. Chem. Soc., Faraday Trans. 2 **73**, 1133 (1977).
[36] M. J. P. Nijmeijer, A. F. Bakker, C. Bruin, and J. H. Sikkenk, J. Chem. Phys. **89**, 3789 (1988).
[37] C. D. Holcomb, P. Clancy, and J. A. Zollweg, Mol. Phys. **78**, 437 (1993).
[38] L. Chen, J. Chem. Phys. **103**, 10214 (1995).
[39] A. Trokhymchuk and J. Aleiandre, J. Chem. Phys. **111**, 8510 (1999).